Mycobacterium abscessus L,D-Transpeptidases Are Susceptible to Inactivation by Carbapenems and Cephalosporins but Not Penicillins

Pankaj Kumar,[a,b] Varsha Chauhan,[a,b] José Rogério A. Silva,[c,d] Jerônimo Lameira,[c,d] Felipe B. d'Andrea,[b] Shao-Gang Li,[e] Stephan L. Ginell,[f] Joel S. Freundlich,[e] Cláudio Nahum Alves,[c,d] Scott Bailey,[g] Keira A. Cohen,[h] Gyanu Lamichhane[a,b]

Center for Tuberculosis Research, Department of Medicine, Johns Hopkins University, Baltimore, Maryland, USA[a]; Taskforce To Study Resistance Emergence and Antimicrobial Development Technology, Department of Medicine, Johns Hopkins University, Baltimore, Maryland, USA[b]; Programa de Pós-Graduação em Química Medicinal e Modelagem Molecular, Instituto de Ciências da Saúde, Universidade Federal do Pará, Belém, Pará, Brazil[c]; Laboratório de Planejamento e Desenvolvimento de Fármacos, Instituto de Ciências Exatas e Naturais, Universidade Federal do Pará, Belém, Pará, Brazil[d]; Departments of Pharmacology, Physiology and Neuroscience, and Medicine, Rutgers University, Newark, New Jersey, USA[e]; Biosciences Division, Argonne National Laboratory, Argonne, Illinois, USA[f]; Department of Biochemistry and Molecular Biology, Bloomberg School of Public Health, Johns Hopkins University, Baltimore, Maryland, USA[g]; Division of Pulmonary and Critical Care Medicine, Brigham and Women's Hospital, Boston, Massachusetts, USA[h]

ABSTRACT As a growing number of clinical isolates of *Mycobacterium abscessus* are resistant to most antibiotics, new treatment options that are effective against these drug-resistant strains are desperately needed. The majority of the linkages in the cell wall peptidoglycan of *M. abscessus* are synthesized by nonclassical transpeptidases, namely, the L,D-transpeptidases. Emerging evidence suggests that these enzymes represent a new molecular vulnerability in this pathogen. Recent studies have demonstrated that inhibition of these enzymes by the carbapenem class of β-lactams determines their activity against *Mycobacterium tuberculosis*. Here, we studied the interactions of β-lactams with two L,D-transpeptidases in *M. abscessus*, namely, Ldt_{Mab1} and Ldt_{Mab2}, and found that both the carbapenem and cephalosporin, but not penicillin, subclasses of β-lactams inhibit these enzymes. Contrary to the commonly held belief that combination therapy with β-lactams is redundant, doripenem and cefdinir exhibit synergy against both pansusceptible *M. abscessus* and clinical isolates that are resistant to most antibiotics, which suggests that dual-β-lactam therapy has potential for the treatment of *M. abscessus*. Finally, we solved the first crystal structure of an *M. abscessus* L,D-transpeptidase, Ldt_{Mab2}, and using substitutions of critical amino acids in the catalytic site and computational simulations, we describe the key molecular interactions between this enzyme and β-lactams, which provide an insight into the molecular basis for the relative efficacy of different β-lactams against *M. abscessus*.

KEYWORDS L,D-transpeptidase, *Mycobacterium abscessus*, beta-lactams, carbapenem, cephalosporin

Address correspondence to Gyanu Lamichhane, lamichhane@jhu.edu.

Mycobacterium abscessus is a rapid-growing nontuberculous mycobacterium that causes a wide range of opportunistic infections in humans (1). Vulnerable populations, including individuals with chronic lung disease, such as cystic fibrosis, are prone to high rates of *M. abscessus* infection (2, 3). Natural and acquired resistance to many antibiotics signifies limited options for the treatment of *M. abscessus* infections (4, 5). Although a comprehensive survey of the current drug resistance profile of clinical isolates of *M. abscessus* is not available, data from 28 strains isolated from cystic fibrosis

patients over the past decade show high levels of resistance to most drugs used to treat this infection clinically (6). A drug that inhibits a novel target and has efficacy against strains with resistance to currently available drugs would provide a means to meet this clinical need.

β-Lactams are a powerful class of antibiotics that are widely used to treat a broad spectrum of bacterial infections. Historically, β-lactams were thought to act by inhibiting only the D,D-transpeptidases (also known as penicillin binding proteins) (7). This enzyme class catalyzes the final step of peptidoglycan biosynthesis in bacteria and forms transpeptide linkages between the fourth and third residues of peptide side chains, designated 4→3 linkages. While the peptidoglycan of *M. abscessus* contains classical 4→3 linkages, the majority of the peptidoglycan linkages are between the third residues of the peptide side chains (8). These linkages also predominate the peptidoglycan of *Mycobacterium tuberculosis* (9–11). These unique 3→3 linkages are generated by nonclassical transpeptidases, namely, L,D-transpeptidases (12). Emerging evidence shows that *M. abscessus* may be more susceptible to carbapenems (13) and that the potency of this β-lactam subclass is driven by its unique ability to inhibit L,D-transpeptidases (14). Currently, cefoxitin (a cephalosporin) and imipenem (a carbapenem) are the only two β-lactam agents that are included in guidelines for the treatment of *M. abscessus*, and between these two drugs, imipenem exhibits higher potency against this mycobacterium (15). A comprehensive study of L,D-transpeptidase interactions with additional β-lactams would yield further insight into the utility of these drugs for the treatment of *M. abscessus* infections.

The genome of *M. abscessus* encodes orthologs of five L,D-transpeptidases present in *M. tuberculosis* (16). In this study, we cloned, expressed, and purified two L,D-transpeptidases from *M. abscessus*, namely, Ldt_{Mab1} and Ldt_{Mab2}, and assessed the abilities of a wide variety of β-lactams to inhibit these enzymes. Next, we evaluated whether the β-lactams that inhibited the L,D-transpeptidases also inhibited the growth of both susceptible and drug-resistant clinical isolates of *M. abscessus*. Additionally, we used X-ray crystallography, computational simulation, and substitutions of critical amino acids involved in the active site to determine molecular interactions between β-lactams and Ldt_{Mab2}.

RESULTS

Carbapenems and cephalosporins inhibit Ldt_{Mab1} and Ldt_{Mab2} to various extents. We measured the relative inhibition of Ldt_{Mab1} and Ldt_{Mab2} activities by a variety of β-lactam antibiotics. The tested β-lactams included penicillins (amoxicillin, ampicillin, carbenicillin, methicillin, and oxacillin), cephalosporins (cefdinir, cefotaxime, cefoxitin, ceftriaxone, and cephalexin), a penem (faropenem), commercially available carbapenems (biapenem, doripenem, ertapenem, imipenem, meropenem, and tebipenem), and novel experimental carbapenems (T202, T203, T205, T206, T210, and T223) (see Fig. S1 in the supplemental material) (14). Nitrocefin, a chromogenic β-lactam that is hydrolyzed by Ldt_{Mab1} and Ldt_{Mab2}, was used as a substrate to monitor the activities of these enzymes in the presence of β-lactams.

Relative inhibition of Ldt_{Mab1}. None of the tested penicillins inhibited Ldt_{Mab1} (Fig. 1a). With the exception of cephalexin, which showed only minimal inhibition, all cephalosporins appeared to inhibit Ldt_{Mab1} to similar degrees (Fig. 1b). Among the carbapenems, while neither meropenem nor imipenem appeared to have an inhibitory effect, the relative order in which the others inhibited Ldt_{Mab1} was biapenem > doripenem = ertapenem > tebipenem (Fig. 1c). Similarly, experimental carbapenems inhibited Ldt_{Mab1} in the order of T205 > T210 = T203 = T223 > T202, while T206 showed no inhibition effect (Fig. 1d). Interestingly, among all the β-lactams tested, faropenem, a penem, inhibited Ldt_{Mab1} to the greatest extent (Fig. 1c).

Relative inhibition of Ldt_{Mab2}. In contrast to Ldt_{Mab1}, all of the tested penicillins exhibited moderate inhibition of Ldt_{Mab2}. The greatest to least inhibition was observed in the following order: carbenicillin = oxacillin = amoxicillin > methicillin = ampicillin (Fig. 1e). Among the cephalosporins, while cephalexin failed to inhibit Ldt_{Mab2}, the
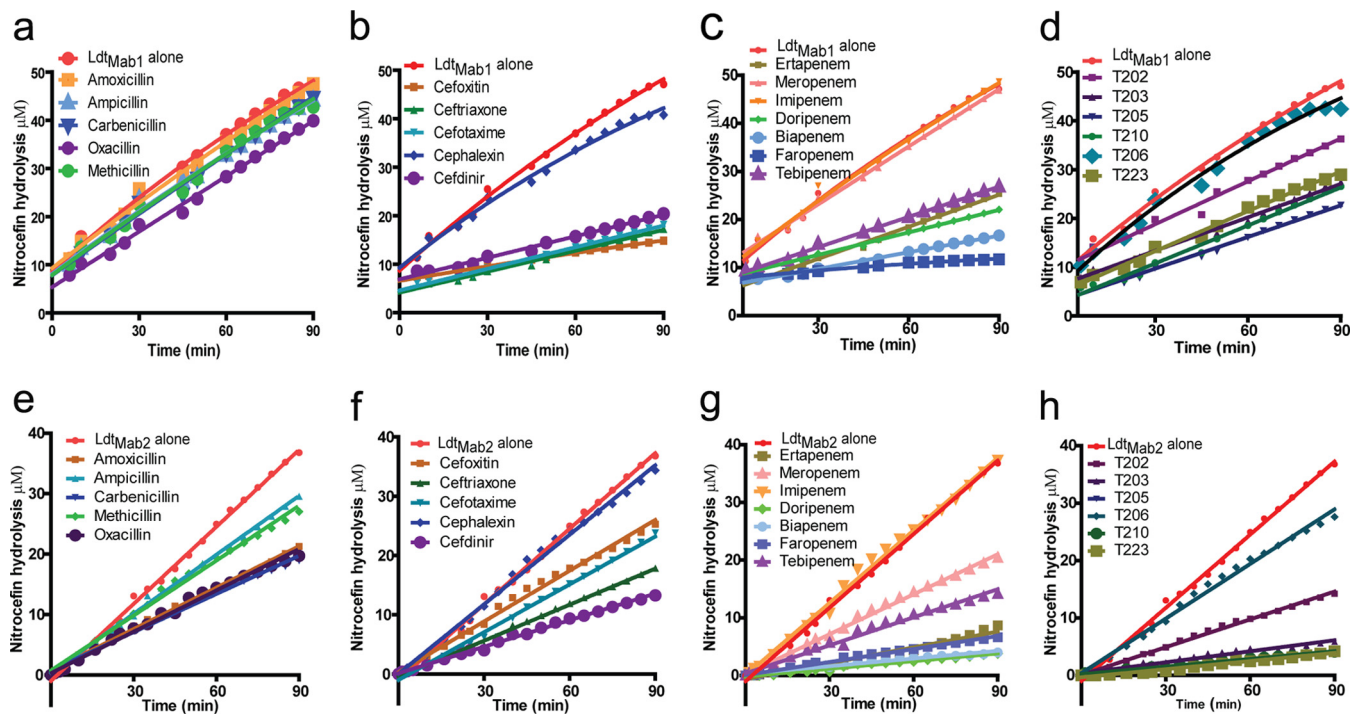
FIG 1 Nitrocefin hydrolysis by Ldt$_{Mab1}$ and Ldt$_{Mab2}$ in the presence of β-lactams. Profiles of nitrocefin hydrolysis by Ldt$_{Mab1}$ in the presence of penicillins (a), cephalosporins (b), commercially available carbapenems and penem (c), and experimental carbapenems (d) and nitrocefin hydrolysis by Ldt$_{Mab2}$ in the presence of penicillins (e), cephalosporins (f), commercially available carbapenems and penem (g), and experimental carbapenems (h) are illustrated.

relative extent to which the others inhibited the enzyme was cefdinir > ceftriaxone > cefotaxime > cefoxitin (Fig. 1f). With the exception of imipenem, the carbapenems were the most potent inhibitors of Ldt$_{Mab2}$, with the following relative inhibition profile: doripenem = biapenem > ertapenem > tebipenem > meropenem (Fig. 1g). Among the experimental carbapenems, T206 showed no inhibition, and the others inhibited the enzyme in the following descending order: T223 = T210 = T205 > T203 > T202 (Fig. 1h). Faropenem, a penem, was also a potent inhibitor of Ldt$_{Mab2}$ (Fig. 1g). As a class, the carbapenems were the most efficient inhibitors of Ldt$_{Mab2}$, with doripenem and biapenem showing the highest degree of inhibition.

Doripenem and cefdinir exhibit synergy against *M. abscessus*. We hypothesized that the combination of a carbapenem and a cephalosporin, the two subclasses of β-lactams that inhibited Ldt$_{Mab1}$ and Ldt$_{Mab2}$ to the greatest extent, may exhibit synergistic activity by targeting enzymes in *M. abscessus* that are differentially susceptible to these β-lactam subclasses. To test this hypothesis, we selected the following carbapenems based on their relative abilities to inhibit Ldt$_{Mab1}$ and Ldt$_{Mab2}$ (Fig. 1a to h): doripenem, biapenem, tebipenem, ertapenem, T205, T210, and faropenem (a penem). Among the cephalosporins, we chose cefdinir, as it was the most potent inhibitor of these enzymes. Drug combinations containing a carbapenem and cefdinir, each at various concentrations, were evaluated in a checkerboard assay against a pansusceptible *M. abscessus* strain, ATCC 19977. The combination of doripenem and cefdinir inhibited *M. abscessus* growth with a fractional inhibitory concentration (FIC) index (FICI) of 0.50, an indication of synergy between these drugs against this bacterium (Table 1). The combination of an experimental carbapenem, T210, and cefdinir was also synergistic against *M. abscessus*, with an FICI of 0.50. The FICI of the combination of biapenem and cefdinir was 0.62, an indication of mild synergy (see Table S1 in the supplemental material).

Next, we assessed whether the combination of doripenem and cefdinir exhibited synergy against clinical isolates of *M. abscessus*. For this task, we chose four strains isolated from cystic fibrosis patients (6), which exhibit a range of resistance against the

TABLE 1 *In vitro* activities of cefdinir and doripenem, alone and in combination, against five *M. abscessus* strains[a]

M. abscessus strain	MIC (μg/ml) against *M. abscessus*		MIC (μg/ml) of cefdinir/MIC (μg/ml) of doripenem against *M. abscessus* (FICI)
	Cefdinir	Doripenem	
ATCC 19977	8–16	4–8	2–4/1–2 (0.5)
1N	8–16	4–8	1–2/2–4 (0.62)
2N	8–16	8–16	1–2/4–8 (0.62)
5N	4–8	4–8	0.25–0.5/2–4 (0.56)
13N	4–8	4–8	0.25–0.5/2–4 (0.56)

[a]MICs of cefdinir and doripenem and FICI values for the combination of cefdinir and doripenem are shown. ATCC 19977 is a reference *M. abscessus* strain, and 1N, 2N, 5N, and 13N are clinical isolates.

antibacterials currently used to treat *M. abscessus* infections (Table S1). Notably, strains 5N and 13N were resistant to imipenem, and strains 1N and 2N displayed intermediate resistance to this carbapenem. The FICI of the combination of doripenem and cefdinir was <1 for all four strains, indicating mild synergy between these two β-lactams against these strains (Table 1). Most interestingly, the reduction of the MIC of doripenem and cefdinir, when used as a combination, is highly significant for therapeutic applications.

Crystal structure of Ldt$_{Mab2}$ provides insight into its inhibition by β-lactams. We hypothesized that the various levels of inhibition of Ldt$_{Mab1}$ and Ldt$_{Mab2}$ by different β-lactams could be attributed to differences in the molecular interactions of the drugs with these enzymes. As each individual β-lactam is unique in structure and chemical composition, the interactions of β-lactams with the enzymes and, consequently, the levels of enzyme inhibition are likely to differ. We determined the crystal structure of Ldt$_{Mab2}$ and performed molecular dynamics studies with select β-lactams to gain insight into the molecular interactions between the drugs and the enzyme. Ldt$_{Mab2}$ was selected for structural studies, as its ortholog Ldt$_{Mt2}$ is the primary L,D-transpeptidase in *M. tuberculosis* (10, 17).

The crystal structure of Ldt$_{Mab2}$ (fragment ΔN41) was solved at a 2.98-Å resolution (see Table S2 in the supplemental material). Electron density was not observed for residues 42 to 55. Therefore, the structure reported corresponds to residues 56 to 406. There are six chains in the asymmetric unit of Ldt$_{Mab2}$. We superposed five chains (chains B, C, D, E, and F) to chain A to calculate their root mean square deviation (RMSD) values along the C$_\alpha$ atoms from residues 56 to 406. Chain B superposed with an RMSD of 0.432 Å, chain C superposed with an RMSD of 0.48 Å, chain D superposed with an RMSD of 0.663 Å, chain E superposed with an RMSD of 0.718 Å, and chain F superposed with an RMSD of 0.969 Å. Superposition of different chains revealed maximum variation along the Cα backbone in the IgD-like domain spanning residues 56 to 144 and in the YkuD domain spanning residues 295 to 322.

We next compared the structure of Ldt$_{Mab2}$ (Fig. 2a) with that of Ldt$_{Mt2}$ (PDB accession number 5DU7) (14). Ldt$_{Mab2}$ superposed to Ldt$_{Mt2}$ along the C$_\alpha$ backbone atoms corresponding to residues 56 to 406 with an RMSD of 1.52 Å. IgD-like domain 1 (18) in the N terminus of Ldt$_{Mab2}$ showed the most conformational differences compared to the corresponding domain in Ldt$_{Mt2}$ (Fig. S2). This suggests that the N-terminal domain of Ldt$_{Mab2}$ is flexible. In the YkuD domain of Ldt$_{Mab2}$, the flap loop (residues 304 to 313) is disordered. The major differences between Ldt$_{Mab2}$ and Ldt$_{Mt2}$ occur in the catalytic domain (Fig. 2b), which belongs to the YkuD family (Pfam 03734). We superposed the YkuD domains of the two enzymes (Fig. 2c) and compared critical structural differences. While the active sites of Ldt$_{Mab2}$ and Ldt$_{Mt2}$ appear structurally similar, there are several differences in amino acids that may affect their ligand specificity and enzymatic activity. Notably, many residues in the inner cavity that are involved in interactions with the side chains of β-lactams (14) are not conserved. These residues are F295, Y331, N285, P380, K281, and A282.

Molecular dynamics simulations of β-lactam binding to Ldt$_{Mab2}$. We made several unsuccessful attempts to cocrystallize Ldt$_{Mab2}$ with β-lactams to gain insight into
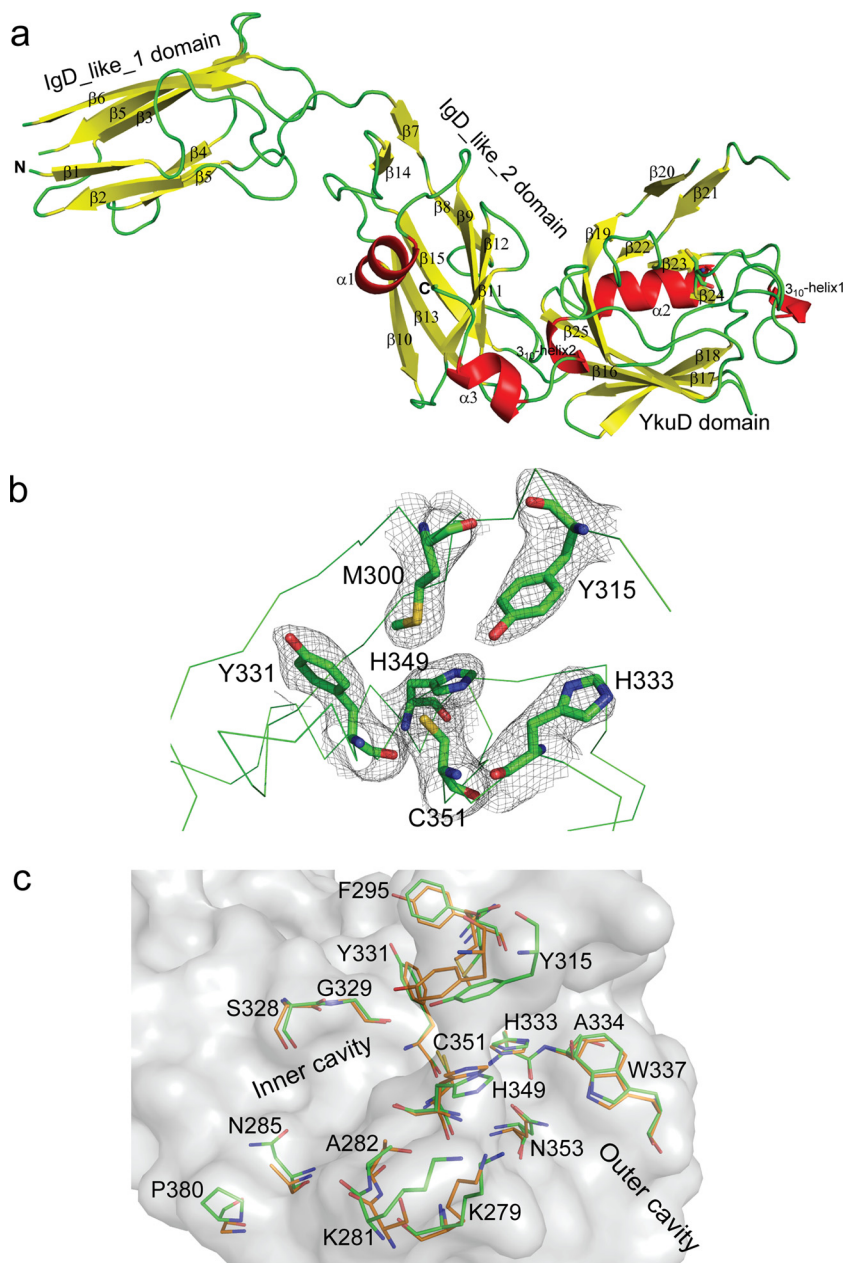
FIG 2 Crystal structure of Ldt$_{Mab2}$. (a) Crystal structure of Ldt$_{Mab2}$ detailing the tertiary structure of the enzyme. (b) Electron density map ($2F_o - F_c$), contoured at 1 σ, of the active site of Ldt$_{Mab2}$. (c) Superposition of L,D-transpeptidase active sites of Ldt$_{Mab2}$ (green) and Ldt$_{Mt2}$ (orange).

molecular interactions between the enzyme and this antibiotic class. As an alternate approach, we performed molecular dynamics simulations of interactions of select β-lactams with the Ldt$_{Mab2}$ active site. Cefdinir, cephalexin, doripenem, and tebipenem were chosen for this analysis, as they represent both weak and strong inhibitors of the enzyme (Fig. 1f and g). These β-lactams were docked into the active site of the experimentally generated three-dimensional (3-D) crystal structure of Ldt$_{Mab2}$ (see Table S3 in the supplemental material). The docked Ldt$_{Mab2}$–β-lactam complexes were used as starting points for molecular dynamics simulations. A total of 100 ns of molecular dynamics simulations was carried out in an explicit water solvent for each Ldt$_{Mab2}$–β-lactam pair. After the initial 30 ns, all pairs were fairly stable during the entire remaining period of the molecular dynamics simulations, with RMSD values, with

**TABLE 2** Thermodynamic parameters that describe binding interactions of Ldt$_{Mab2}$ with β-lactams[a]

β-Lactam	E_{vdW} (kcal · mol^{-1})	E_{elec} (kcal · mol^{-1})	G_{GB} (kcal · mol^{-1})	$G_{nonpolar}$ (kcal · mol^{-1})	ΔG_{bind} (kcal · mol^{-1})
Cefdinir	−39.81	−71.81	89.17	−4.69	−27.14
Cephalexin	−27.80	−72.35	83.24	−5.20	−22.11
Doripenem	−43.64	−58.95	69.36	−5.15	−38.38
Tebipenem	−44.26	−52.44	69.26	−4.96	−32.40

[a]Free energy of the binding (ΔG_{bind}) of β-lactams to Ldt$_{Mab2}$ calculated from van der Waals interactions (E_{vdW}), electrostatic interactions (E_{elec}), and polar (G_{GB}) and nonpolar ($G_{nonpolar}$) contributions.

respect to the average structure, of 1.14 ± 0.31, 1.49 ± 0.28, 1.38 ± 0.33, and 1.18 ± 0.35 for cefdinir, cephalexin, doripenem, and tebipenem, respectively (Fig. S3). In addition, we calculated the binding energies for the Ldt$_{Mab2}$–β-lactam pairs using the final 20 ns of molecular dynamics simulations for a total of 2,000 snapshots (Table 2). Carbapenems consistently exhibited lower binding free energy (ΔG_{bind}) than the cephalosporins, indicating that they bind more tightly with Ldt$_{Mab2}$. Between the two carbapenems tested, ΔG_{bind} values were lowest for doripenem and highest for tebipenem. Therefore, doripenem binds more tightly than tebipenem to Ldt$_{Mab2}$. These data are concordant with the relative strengths with which doripenem and tebipenem inhibit the activity of Ldt$_{Mab2}$, as observed in the nitrocefin hydrolysis assay (Fig. 1g). Between the two cephalosporins, the lower ΔG_{bind} value for cefdinir indicates that it binds more tightly than cephalexin to Ldt$_{Mab2}$, again in agreement with data from the nitrocefin hydrolysis inhibition assay, where cefdinir exhibited higher potency and cephalexin exhibited the lowest potency (Fig. 1f).

Interactions between β-lactams and the residues in the active site of L,D-transpeptidases affect the overall inhibition of these enzymes (14). To further understand the relevance of specific residues in the active site of Ldt$_{Mab2}$ for binding to β-lactams, the average binding free energies of decomposition for relevant residues were measured against their interactions with cefdinir, cephalexin, doripenem, and tebipenem (Fig. 3). These β-lactams interacted with residues M300, Y305, Y315, S348, H349, G350, and C351, and their interactions exhibited a range of free energies (Table S4). Cefdinir made additional interactions with residues T304, G329, and Y331 (Fig. 3a). While T304 is part of the active-site flap, G329 and Y331 are located in the inner cavity of the active site of Ldt$_{Mab2}$ (Fig. 2b and c). In the molecular dynamics simulations, the 100 ns snapshot shows that the 2-aminothiazole of the R2 side chain of cefdinir makes hydrogen bond interactions with these residues (Fig. S4). Unlike cefdinir, cephalexin exhibited low binding energies with active-site residues T304, G329, and Y331 but exhibited additional interactions with outer cavity residues W337 and N353, residue V319 in the active-site flap, and residue H333 in the catalytic core (Fig. 2b and c and 3b). While most of the interactions of doripenem and tebipenem with Ldt$_{Mab2}$ were similar, the two carbapenems made critically different interactions with residues T304, Y315, and R316 (Fig. 3c and d and Table S4).
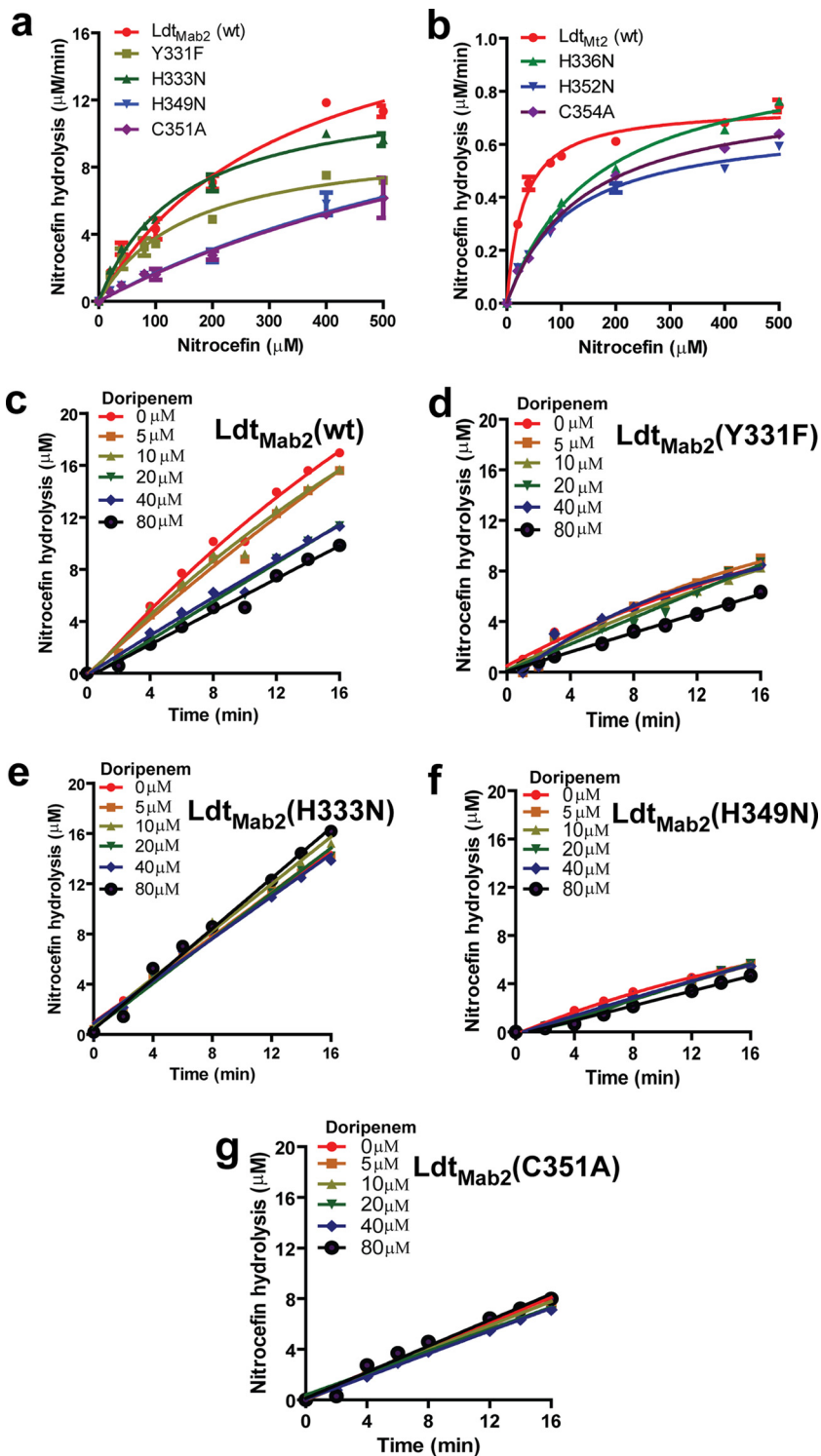
Role of Ldt$_{Mab2}$ active-site residues in β-lactam ring hydrolysis. Guided by the crystal structure and molecular dynamics studies, we selected residues in the active site of Ldt$_{Mab2}$ that make critical interactions with β-lactams to further assess their contributions to the overall enzyme activity. For this task, we generated Ldt$_{Mab2}$ with the following amino acid substitutions: Y331F, H333N, H349N, and C351A. We observed that these mutants hydrolyzed nitrocefin at varying rates (Fig. 4a). Somewhat surprisingly, the C351A mutant hydrolyzed nitrocefin with the same V_{max} as that of wild-type Ldt$_{Mab2}$, although the mutant showed an ~3-fold-higher K_m for nitrocefin (Table 3). The H349N mutant also showed an ~3-fold increase in the K_m for nitrocefin. For the Y331F and H333N mutants, while the V_{max} decreased, the K_m did not change significantly. Next, we investigated whether the phenomenon of nitrocefin β-lactam ring hydrolysis in the absence of catalytically important residues also occurred with Ldt$_{Mt2}$, the ortholog of Ldt$_{Mab2}$ in *M. tuberculosis*. Based on the alignment of the amino acid
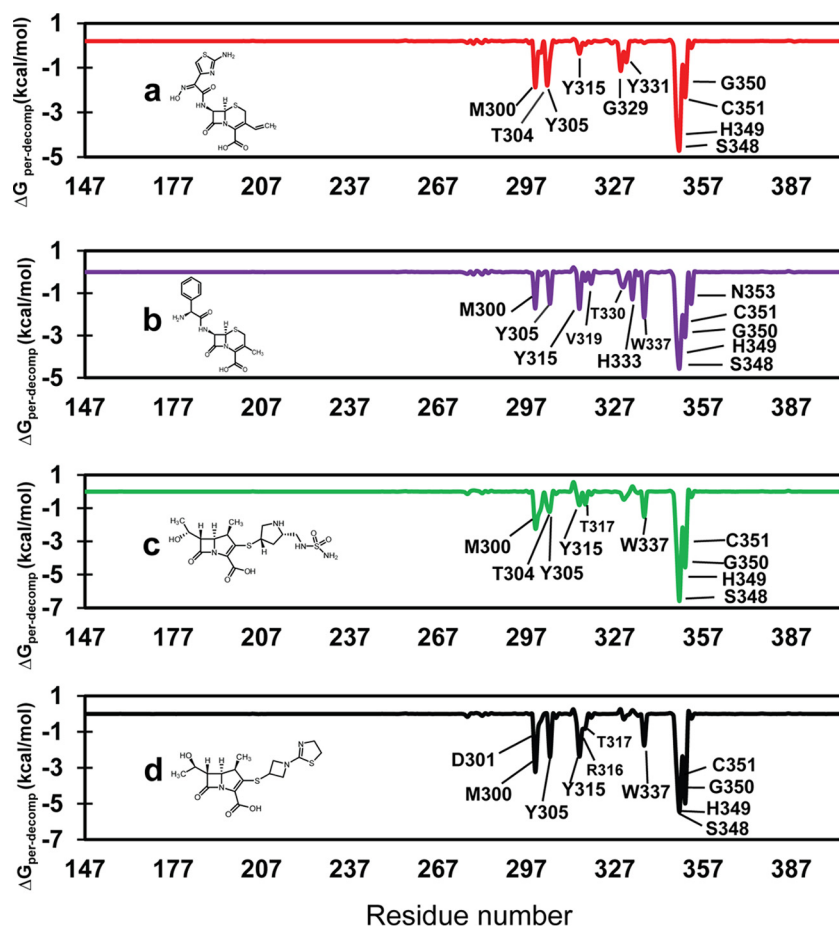
FIG 3 Profile of binding free energies contributed by each residue to stabilize the Ldt_{Mab2}–β-lactam complex. Residues with $\Delta G_{\text{per-decomp}}$ values of $\geq$0.5 kcal/mol are labeled. Per-decomp refers to per residual decomposition. (a) Ldt_{Mab2}-cefdinir; (b) Ldt_{Mab2}-cephalexin; (c) Ldt_{Mab2}-doripenem; (d) Ldt_{Mab2}-tebipenem.

sequences of these enzymes (Fig. S5), we generated similar active-site mutants in Ldt_{Mt2}: H336N (corresponding to H333N in Ldt_{Mab2}), H352N (corresponding to H349N in Ldt_{Mab2}), and C354A (corresponding to C351A in Ldt_{Mab2}). These Ldt_{Mt2} mutants hydrolyzed nitrocefin with similar V_{max} values but with an increased K_m (Fig. 4b).

We expected cysteine (C351 in Ldt_{Mab2} and the corresponding residue C354 in Ldt_{Mt2}) mutants to be catalytically inactive, as this amino acid is directly involved in β-lactam ring opening in carbapenems (14). The binding of a β-lactam to an L,D-transpeptidase has been proposed to follow three steps (19): initial noncovalent binding followed by the acylation of the catalytic cysteine and the subsequent hydrolysis of the acyl complex. The rates of the final step can vary significantly among different β-lactam classes and L,D-transpeptidases. For instance, with Ldt_{Mt2} and carbapenems, this rate is very low, and stable acyl adducts are detected even after 24 h (14). $\text{Ldt}_{\text{Mab2}}{}^{\text{C351A}}$ and $\text{Ldt}_{\text{Mt2}}{}^{\text{C354A}}$ were able to hydrolyze nitrocefin albeit at a reduced rate (Fig. 4a and b). There is a precedent for β-lactam ring hydrolysis without the involvement of a catalytic residue. It has been speculated that a water molecule in the active site of the β-lactamase TEM-1 with a catalytic serine substitution can act as a nucleophile and open the β-lactam ring (20). Therefore, it is possible that nitrocefin reacts with water at the catalytic site. Histidine in the active site of Ldt_{Mt2} facilitates the protonation of the β-lactam ring nitrogen (14). As the H333N mutant (and $\text{Ldt}_{\text{Mt2}}{}^{\text{H336N}}$) was able to hydrolyze nitrocefin (Fig. 4a and b), the existence of an alternate proton donor is likely. A recent study suggested a role of water in the protonation of the β-lactam ring nitrogen in Ldt_{Mt2} (21).

FIG 4 Role of L,D-transpeptidase active-site amino acid residues in β-lactam hydrolysis and inhibition by doripenem. (a) Kinetics of nitrocefin hydrolysis by Ldt$_{Mab2}$ wild-type (wt) and mutant proteins. (b) Kinetics of nitrocefin hydrolysis by Ldt$_{Mt2}$ wild-type and mutant proteins. (c to g) Inhibition of the nitrocefin hydrolysis activity of Ldt$_{Mab2}$ wild-type and mutant proteins by doripenem at various concentrations.

Next, we used doripenem, a carbapenem, to probe the involvement of Y331, H333, H349, and C351 in Ldt$_{Mab2}$, as the corresponding residues in Ldt$_{Mt2}$ are critical for reactions with carbapenems (14). As expected, a gradual decrease in nitrocefin hydrolysis with increasing concentrations of doripenem was observed with wild-type Ldt$_{Mab2}$

TABLE 3 Kinetic parameters of nitrocefin hydrolysis by Ldt_{Mab2} and Ldt_{Mt2}[a]

Enzyme	Mean V_{max} (μM/min) $\pm$ SD	Mean K_m (μM) $\pm$ SD
Ldt_{Mab2}^{wt}	19.8 $\pm$ 2.03	328.3 $\pm$ 65.5
Ldt_{Mab2}^{Y331F}	9.7 $\pm$ 0.6	155.7 $\pm$ 25.8
Ldt_{Mab2}^{H333N}	12.9 $\pm$ 0.5	147.5 $\pm$ 15.0
Ldt_{Mab2}^{H349N}	18.8 $\pm$ 5.3	1,010 $\pm$ 395
Ldt_{Mab2}^{C351A}	18.6 $\pm$ 5.8	1,022 $\pm$ 441
Ldt_{Mt2}^{wt}	0.74 $\pm$ 0.02	30.0 $\pm$ 2.9
Ldt_{Mt2}^{H336N}	0.96 $\pm$ 0.03	163.3 $\pm$ 14.4
Ldt_{Mt2}^{H352N}	0.69 $\pm$ 0.02	115.7 $\pm$ 11.1
Ldt_{Mt2}^{C354A}	0.81 $\pm$ 0.02	140.8 $\pm$ 6.9

[a]wt, wild type.

(Fig. 4c). However, the nitrocefin hydrolysis activities of the H333N, H349N, and C351A mutants were not altered by doripenem (Fig. 4d to g). This observation confirms that these residues are involved in interactions with doripenem.

DISCUSSION

In this study, we determined the relative inhibition of the *M. abscessus* L,D-transpeptidases Ldt_{Mab1} and Ldt_{Mab2} by different classes of β-lactams and determined the MICs of the β-lactams against *M. abscessus* that were the most potent inhibitors of these critical enzymes. Interestingly, we observed that combinations of β-lactams from different classes exhibit synergy against *M. abscessus*, which suggests broader clinical application of dual-β-lactam therapy. Finally, we determined the first crystal structure of a key *M. abscessus* transpeptidase, Ldt_{Mab2}; performed molecular dynamics studies that predicted binding affinities of various β-lactams; and performed enzymatic assays with active-site mutants of Ldt_{Mab2} that provided an insight into the molecular interactions of this enzyme with β-lactams.

The genome of *M. abscessus* encodes orthologs of five L,D-transpeptidases present in *M. tuberculosis* (10, 16). As none of the orthologs in *M. abscessus* have been characterized, here, we chose to focus on Ldt_{Mab2}, as its ortholog in *M. tuberculosis*, Ldt_{Mt2}, is the dominant L,D-transpeptidase, and its loss renders *M. tuberculosis* susceptible to amoxicillin-clavulanate (10). Ldt_{Mab2} and Ldt_{Mt2} share 80% amino acid sequence similarity (see Fig. S5 in the supplemental material).

We hypothesized that the mechanism of β-lactam ring opening of nitrocefin by Ldt_{Mab2} would be similar to the proposed β-lactam ring opening in carbapenems and penems by Ldt_{Mt2} (14, 22). This mechanism proposed the roles of cysteine (C351 in Ldt_{Mab2}) and histidine (H333 in Ldt_{Mab2}) residues in β-lactam ring opening and acylation, where the cysteine acts as a nucleophile and subsequently becomes acylated by the carbonyl carbon of the β-lactam ring. Simultaneously, the histidine protonates the β-lactam ring nitrogen. However, nitrocefin hydrolysis by Ldt_{Mab2} C351A and H333N substitution mutants suggests that the opening of the β-lactam ring in nitrocefin does not follow the same mechanism and potentially involves bulk water present in the catalytic site or involves another residue. Nitrocefin is a cephalosporin, a β-lactam subclass with a chemical composition that is distinct from those of carbapenems and penems. It is likely that the interaction of cephalosporins with an L,D-transpeptidase is distinct from those of other β-lactam subclasses.

Optimization of β-lactam selection for inclusion in regimens holds significant untapped potential for the clinical treatment of *M. abscessus* infections. Current *M. abscessus* treatment guidelines include only two β-lactams: cefoxitin (a cephalosporin) and imipenem (a carbapenem) (23). However, we observed only a modest ability of these agents to inhibit Ldt_{Mab1} and Ldt_{Mab2}, whereas other β-lactams were much more potent inhibitors of these enzymes (Fig. 1). In particular, faropenem (a penem), biapenem, and doripenem (both carbapenems) showed exceptional abilities to inhibit both Ldt_{Mab1} and Ldt_{Mab2}. Among cephalosporins, cefdinir (an oral agent) was observed to have the greatest inhibition of Ldt_{Mab2}. While some of these potent agents (for

example, biapenem and faropenem) are not currently available in the United States, doripenem is FDA approved and holds promise for clinical use against *M. abscessus*.

Of note, several novel experimental carbapenems newly synthesized by our laboratory (14), including T205 and T223, showed inhibition of Ldt$_{Mab1}$ and Ldt$_{Mab2}$, respectively (Fig. 1). These promising novel agents merit further study to define their safety, efficacy, and potential for further drug development for use against *M. abscessus*.

Our study is the first to demonstrate that combinations of dual β-lactams exhibit synergy against *M. abscessus*. This synergy is likely attributed to nonredundant targets and the differential inhibition of both nonclassical (Ldt$_{Mab1}$ and Ldt$_{Mab2}$) and classical (D,D-transpeptidases) transpeptidases, a concept which to date has been underappreciated and underexplored in mycobacteria. An antimycobacterial regimen that contains only a single β-lactam agent may not fully inhibit mycobacterial peptidoglycan synthesis, which in turn may prevent full antimicrobial killing that occurs when this key pathway is effectively shut down. In particular, the combination of doripenem and cefdinir was synergistic and very potent against *M. abscessus* (Table 1), and this combination should be considered for further preclinical development for this pathogen. Importantly, dual-agent synergy was observed with both the key laboratory strain ATCC 19977 and multiple-drug-resistant clinical isolates, which shows the potential for dual-β-lactam therapy to revolutionize the design of antimycobacterial clinical regimens. Synergy of dual β-lactams against *M. tuberculosis* and *Enterococcus faecalis* was recently observed by two different groups (24, 25).

Importantly, a significant degree of intrinsic resistance to β-lactams in *M. abscessus* is conferred by a chromosomally encoded highly active class A β-lactamase, Bla$_{Mab}$ (26). Bla$_{Mab}$ inactivates both β-lactams and β-lactamase inhibitors with the β-lactam chemical nucleus (for example, clavulanate and sulbactam). Surprisingly, compared to penicillins and carbapenems, cephalosporins are more resistant to hydrolysis by Bla$_{Mab}$ (26). Among β-lactamase inhibitors, Bla$_{Mab}$ is effectively inhibited by avibactam, a non-β-lactam agent (27), and the addition of avibactam to carbapenems has shown promise *in vitro* against *M. abscessus* (6, 28). We anticipate that even more profound synergy would be observed with the addition of avibactam to a dual-β-lactam regimen. In the future, we intend to examine the potential of avibactam and other β-lactamase inhibitors to further enhance the potency of dual-β-lactam regimens.

MATERIALS AND METHODS

Bacterial strains, growth media, and drugs. *Mycobacterium abscessus* ATCC 19977 was used as the primary strain. In addition, four *M. abscessus* clinical strains isolated from cystic fibrosis patients, labeled 1N, 2N, 5N, and 13N, were used for MIC determinations. All strains were grown in Middlebrook 7H9 broth with albumin-dextrose-catalase enrichment with constant shaking at 37°C. β-Lactams (amoxicillin, ampicillin, carbenicillin, methicillin, oxacillin, cefoxitin, ceftriaxone, cefotaxime, cephalexin, cefdinir, ertapenem, meropenem, imipenem, doripenem, biapenem, faropenem, and tebipenem) were procured from a commercial vendor (Sigma-Aldrich). The following novel experimental carbapenems synthesized by our group were also tested: T202, T203, T205, T206, T210, and T223 (14).

Cloning, expression, and purification of proteins. The amino acid sequences of the L,D-transpeptidases of *M. tuberculosis*, namely, Ldt$_{Mt1}$ and Ldt$_{Mt2}$ (9, 10), were used to identify orthologs in *M. abscessus* by using a BLAST search. These respective orthologs, MAB_3165c and MAB_1530, are referred to here as Ldt$_{Mab1}$ and Ldt$_{Mab2}$, respectively. A putative transmembrane domain, similar to that in Ldt$_{Mt2}$ (29), exists in Ldt$_{Mab2}$. During cloning, this domain was excluded and only the fragment containing residues 42 to 406 (ΔN41) was included to facilitate the overexpression and purification of the soluble protein. The corresponding gene fragment from *M. abscessus* ATCC 19977 was cloned into the multiple-cloning site in pET28a$^+$ with an N-terminal His$_6$ tag that can be removed with tobacco etch virus (TEV) protease (29). Proteins were overexpressed and purified as follows. *Escherichia coli* BL21δε3 (catalog number C2527H; NEB Labs) cells transformed with a pET28a$^+$ vector carrying the desired gene fragments were grown in Luria-Bertani (LB) medium at 37°C to exponential phase (culture A_{600} of ~0.8), induced with 0.25 mM isopropyl-β-D-1-thiogalactopyranoside (IPTG), and grown overnight at 16°C at 220 rpm with orbital shaking before harvesting by centrifugation. The cells were lysed by sonication in a buffer containing 50 mM Tris (pH 8.0), 400 mM sodium chloride, 1 mM phenylmethanesulfonyl fluoride (PMSF), and 1 mM Tris (2-carboxyethyl) phosphine hydrochloride (TCEP) and centrifuged to separate the soluble protein. The supernatant was passed through a 5-ml HisTrap HP nickel affinity column (GE Healthcare Life Sciences) preequilibrated with wash buffer containing 50 mM Tris (pH 8), 400 mM sodium chloride, 1 mM TCEP, and 0.1 mM PMSF. After the column was washed with 25 column volumes of wash buffer, the bound protein was eluted with a gradient of 1 to 1,000 mM imidazole. The His$_6$ tag was removed from Ldt$_{Mab2}$ by overnight incubation with 2 mg of TEV protease at 4°C while dialyzing the protein against a buffer

containing 50 mM Tris (pH 8), 150 mM sodium chloride, 0.5 mM TCEP, and 0.1 mM PMSF. This mixture was then passed over the nickel affinity column to remove the His$_6$ tag, the remaining uncleaved fusion protein, and the His$_6$-tagged TEV protease. Fractions containing Ldt$_{Mab2}$ were pooled, further purified on a Superdex 200 16/60 column (GE Life Sciences), concentrated up to 30 mg/ml by using a 10,000-molecular-weight-cutoff (MWCO) Vivaspin 20 concentrator, and stored at −80°C. The Ldt$_{Mab1}$ fragment containing residues 32 to 248 (ΔN31) was also cloned, expressed, and purified in a similar manner. The N-terminal 31 residues in Ldt$_{Mab1}$ that encompass a putative transmembrane domain were excluded to facilitate the overexpression and purification of the soluble protein.

Site-directed mutagenesis. Single-amino-acid substitutions of Ldt$_{Mab2}$ (fragment ΔN41) were constructed by site-directed mutagenesis as described previously (30). Briefly, the following primers were used to generate the indicated amino acid substitutions: GTCGTACAGCGGTATT*TTC*GTGCACGCGGCACCG and CGGTGCCGCGTGCAC*GAA*AATACCGCTGTACGAC for Y331F, CAGCGGTATTTACGTG*AAT*GCGGCACCGT GGTCCG and CGGACCACGGTGCCGC*ATT*CACGTAAATACCGCTG for H333N, GCGCACCAACACCAGC*AAT*G GCTGCTTGAACGTCAG and CTGACGTTCAAGCAGCC*ATT*GCTGGTGTTGGTGCGC for H349N, and CAACA CCAGCCACGGC*GCG*TTGAACGTCAGCACGGC and GCCGTGCTGACGTTCAA*CGC*GCCGTGGCTGGTGTTG for C351A (the sequence representing the mutagenized codon is in italic type in each sequence). For each mutagenesis procedure, two separate PCR mixtures, with a forward or reverse primer, NEB fusion polymerase, and high-fidelity buffer, were used on a pET28a$^+$ vector carrying the wild-type sequence for Ldt$_{Mab2}$ (fragment ΔN41) as the template. DNAs from the two reactions were purified, combined, denatured at 95°C, slowly renatured to 37°C, and digested with DpnI. This DNA was used to transform *E. coli* DH5α (catalog number C2987H; NEB Labs), and the plasmid harboring the desired mutation was purified. *E. coli* BL21δε3 (catalog number C2527H; NEB Labs) was used to overproduce proteins.

Nitrocefin hydrolysis assays. Nitrocefin (CalBioChem) is a chromogenic β-lactam whose native and hydrolyzed forms can be monitored at 496 nm. Ldt$_{Mab1}$ and Ldt$_{Mab2}$, each at 10 μM, were reacted with 100 μM nitrocefin in a 100-μl reaction mixture volume at room temperature in a solution containing 25 mM HEPES-morpholineethanesulfonic acid (MES)-diethanolamine and 300 mM NaCl (pH 5.0). Nitrocefin hydrolysis was monitored by using a microplate reader (Bio-Rad). The concentration (c) of hydrolyzed nitrocefin was calculated from its absorbance (A), molar extinction coefficient (ε) (20,500) and path length (l) (0.5 cm) values by using Beer's law: $A = \varepsilon cl$. To assess nitrocefin hydrolysis by Ldt$_{Mab1}$ and Ldt$_{Mab2}$ in the presence of β-lactams, these proteins were added, in separate reaction mixtures at a 10 μM final concentration, to a reaction mixture containing 100 μM nitrocefin and 200 μM various β-lactams. The amount of hydrolyzed nitrocefin was then determined spectroscopically as described previously (14). Nitrocefin in buffer alone (without enzyme) was included to correct for the low level of non-enzyme-driven hydrolysis of nitrocefin.

Crystallization of Ldt$_{Mab2}$. Crystals of Ldt$_{Mab2}$ (ΔN42) were grown by using the sitting-drop vapor diffusion method at 20°C in a solution containing 13% polyethylene glycol 8000 (PEG 8000) and 110 mM sodium citrate tribasic dihydrate (pH 5.5). The crystals appeared in 4 to 5 days and grew to their final size within 3 to 4 weeks. Crystals were flash-frozen and stored in liquid N$_2$ until use.

Data collection and structure determination. X-ray diffraction data were collected at a wavelength of 1.03 Å at beamline 19-ID at the Advanced Photon Source (Argonne National Laboratories). The diffraction data were recorded with a Pilatus3 detector and processed with HKL3000 (31). The Ldt$_{Mab2}$ crystal belongs to the primitive monoclinic space group P2$_1$, with 6 molecules in the asymmetric unit. The crystal structure of Ldt$_{Mab2}$ was solved by the molecular replacement method using PHASER-MR (32) in the PHENIX suite of programs. The coordinates of the *M. tuberculosis* protein Ldt$_{Mt2}$ (PDB accession number 5DU7) were used as a template. The initial density modification, model building, and refinement were performed by using AutoBuild (33), subjected to multiple rounds of crystallographic refinement with phenix.refine from the Phenix suite of programs (34), and rebuilt to fit the electron density with COOT (35). The final model of Ldt$_{Mab2}$ has an R factor value of 20.37% and an R_{free} value of 27.09% for all data between 47.08- and 2.98-Å resolutions. The crystallographic parameters and final refinement statistics are summarized in Table S2. Structure figures were prepared by using the PyMOL Molecular Graphics System, version 1.5.0.4 (Schrödinger, LLC).

Molecular docking, molecular dynamics, and analysis of binding free energy. The crystal structure of Ldt$_{Mab2}$ was used as the starting point for docking and molecular dynamics simulations. The initial docking of cefdinir, cephalexin, doripenem, and tebipenem with Ldt$_{Mab2}$ was performed by using Molegro Virtual Docker (MVD) software (36). Docked results were visually inspected to ensure that an acceptable drug-enzyme interaction was present. The docked Ldt$_{Mab2}$-inhibitor complexes were used as starting structures for the classical molecular dynamics simulations. The simulations performed here were similar to the procedures applied previously to the L,D-transpeptidase Ldt$_{Mt2}$ of *M. tuberculosis* (37).

MIC and fractional inhibitory concentration. A standard broth microdilution method (38) was used to determine the MIC of β-lactams against *M. abscessus* strains. Briefly, an *M. abscessus* culture grown to exponential phase (A_{600} of ~0.5 to 0.6) was used to inoculate ~10^5 bacilli into each well of microtiter culture plates containing a β-lactam in 2-fold serial dilutions with concentrations ranging from 128 to 0.5 μg/ml. The *M. abscessus* cell pellet size was recorded by visual inspection after 3 days of incubation at 30°C without shaking, according to CLSI guidelines (39). The MIC is the lowest concentration of the drug at which an *M. abscessus* cell pellet could not be observed. The checkerboard titration assay, a modification of the broth dilution assay, was used to determine the fractional inhibitory concentration (FIC) of each β-lactam in a combination, as described previously (40). Briefly, two β-lactams, each starting at a concentration equal to its MIC and serially diluted 2-fold, were added to wells in a microtiter culture plate. In this setup, all possible 2-fold dilution combinations up to 1/32 the MIC of each drug were included. An *M. abscessus* culture grown to exponential phase (A_{600} of ~0.5 to 0.6) was used to inoculate

~10^5 bacilli into the wells. The mixtures were incubated at 30°C, and cell pellet sizes were recorded after 3 days. The FIC of each drug and the FIC index (the sum of the FICs of each drug in the combination) were calculated as described previously (40). The final MIC and FIC data represent the averages of results from two biological replicates.

Accession number(s). Coordinates and structure factors have been submitted to the PDB under accession number 5UWV.

SUPPLEMENTAL MATERIAL

Supplemental material for this article may be found at https://doi.org/10.1128/AAC .00866-17.

SUPPLEMENTAL FILE 1, PDF file, 1.3 MB.

ACKNOWLEDGMENTS

REFERENCES

1. Griffith DE, Aksamit T, Brown-Elliott BA, Catanzaro A, Daley C, Gordin F, Holland SM, Horsburgh R, Huitt G, Iademarco MF, Iseman M, Olivier K, Ruoss S, von Reyn CF, Wallace RJ, Jr, Winthrop K. 2007. An official ATS/IDSA statement: diagnosis, treatment, and prevention of nontuberculous mycobacterial diseases. Am J Respir Crit Care Med 175:367–416. https://doi.org/10.1164/rccm.200604-571ST.

2. Olivier KN, Weber DJ, Wallace RJ, Jr, Faiz AR, Lee JH, Zhang Y, Brown-Elliot BA, Handler A, Wilson RW, Schechter MS, Edwards LJ, Chakraborti S, Knowles MR, Nontuberculous Mycobacteria in Cystic Fibrosis Study Group. 2003. Nontuberculous mycobacteria. I. Multicenter prevalence study in cystic fibrosis. Am J Respir Crit Care Med 167:828–834. https://doi.org/10.1164/rccm.200207-678OC.

3. Leung JM, Olivier KN. 2013. Nontuberculous mycobacteria: the changing epidemiology and treatment challenges in cystic fibrosis. Curr Opin Pulm Med 19:662–669. https://doi.org/10.1097/MCP.0b013e328365ab33.

4. Nessar R, Cambau E, Reyrat JM, Murray A, Gicquel B. 2012. Mycobacterium abscessus: a new antibiotic nightmare. J Antimicrob Chemother 67:810–818. https://doi.org/10.1093/jac/dkr578.

5. Benwill JL, Wallace RJ, Jr. 2014. Mycobacterium abscessus: challenges in diagnosis and treatment. Curr Opin Infect Dis 27:506–510. https://doi .org/10.1097/QCO.0000000000000104.

6. Kaushik A, Gupta C, Fisher S, Story-Roller E, Galanis C, Parrish N, Lamichhane G. 16 February 2017. Combinations of avibactam and carbapenems exhibit enhanced potencies against drug-resistant Mycobacterium abscessus. Future Microbiol https://doi.org/10.2217/fmb-2016-0234.

7. Walsh C, Wencewicz TA. 2016. Antibiotics: challenges, mechanisms, opportunities, p 37–68. ASM Press, Washington, DC.

8. Lavollay M, Fourgeaud M, Herrmann JL, Dubost L, Marie A, Gutmann L, Arthur M, Mainardi JL. 2011. The peptidoglycan of Mycobacterium abscessus is predominantly cross-linked by L,D-transpeptidases. J Bacteriol 193:778–782. https://doi.org/10.1128/JB.00606-10.

9. Lavollay M, Arthur M, Fourgeaud M, Dubost L, Marie A, Veziris N, Blanot D, Gutmann L, Mainardi JL. 2008. The peptidoglycan of stationary-phase Mycobacterium tuberculosis predominantly contains cross-links generated by L,D-transpeptidation. J Bacteriol 190:4360–4366. https://doi.org/ 10.1128/JB.00239-08.

10. Gupta R, Lavollay M, Mainardi JL, Arthur M, Bishai WR, Lamichhane G. 2010. The Mycobacterium tuberculosis protein Ldt$_{Mt2}$ is a nonclassical transpeptidase required for virulence and resistance to amoxicillin. Nat Med 16:466–469. https://doi.org/10.1038/nm.2120.

11. Kumar P, Arora K, Lloyd JR, Lee IY, Nair V, Fischer E, Boshoff HI, Barry CE, III. 2012. Meropenem inhibits D,D-carboxypeptidase activity in Mycobacterium tuberculosis. Mol Microbiol 86:367–381. https://doi.org/10.1111/j .1365-2958.2012.08199.x.

12. Mainardi JL, Fourgeaud M, Hugonnet JE, Dubost L, Brouard JP, Ouazzani J, Rice LB, Gutmann L, Arthur M. 2005. A novel peptidoglycan cross-linking enzyme for a β-lactam-resistant transpeptidation pathway. J Biol Chem 280:38146–38152. https://doi.org/10.1074/jbc.M507384200.

13. Kaushik A, Makkar N, Pandey P, Parrish N, Singh U, Lamichhane G. 2015. Carbapenems and rifampin exhibit synergy against Mycobacterium tuberculosis and Mycobacterium abscessus. Antimicrob Agents Chemother 59:6561–6567. https://doi.org/10.1128/AAC.01158-15.

14. Kumar P, Kaushik A, Lloyd EP, Li SG, Mattoo R, Ammerman NC, Bell DT, Perryman AL, Zandi TA, Ekins S, Ginell SL, Townsend CA, Freundlich JS, Lamichhane G. 2017. Non-classical transpeptidases yield insight into new antibacterials. Nat Chem Biol 13:54–61. https://doi.org/10.1038/ nchembio.2237.

15. Lefebvre AL, Dubee V, Cortes M, Dorchene D, Arthur M, Mainardi JL. 2016. Bactericidal and intracellular activity of β-lactams against Mycobacterium abscessus. J Antimicrob Chemother 71:1556–1563. https://doi .org/10.1093/jac/dkw022.

16. Mattoo R, Lloyd EP, Kaushik A, Kumar P, Brunelle JL, Townsend C,

Lamichhane G. 2017. LdtMav2, a non-classical transpeptidase and susceptibility of *Mycobacterium avium* to carbapenems. Future Microbiol 12:595–607. https://doi.org/10.2217/fmb-2016-0208.

17. Schoonmaker MK, Bishai WR, Lamichhane G. 2014. Nonclassical transpeptidases of *Mycobacterium tuberculosis* alter cell size, morphology, the cytosolic matrix, protein localization, virulence, and resistance to *β*-lactams. J Bacteriol 196:1394–1402. https://doi.org/10.1128/JB.01396-13.

18. Marchler-Bauer A, Bo Y, Han L, He J, Lanczycki CJ, Lu S, Chitsaz F, Derbyshire MK, Geer RC, Gonzales NR, Gwadz M, Hurwitz DI, Lu F, Marchler GH, Song JS, Thanki N, Wang Z, Yamashita RA, Zhang D, Zheng C, Geer LY, Bryant SH. 2017. CDD/SPARCLE: functional classification of proteins via subfamily domain architectures. Nucleic Acids Res 45:D200–D203. https://doi.org/10.1093/nar/gkw1129.

19. Lecoq L, Bougault C, Hugonnet JE, Veckerle C, Pessey O, Arthur M, Simorre JP. 2013. Dynamics induced by *β*-lactam antibiotics in the active site of *Bacillus subtilis* L,D-transpeptidase. Structure 20:850–861. https://doi.org/10.1016/j.str.2012.03.015.

20. Stec B, Holtz KM, Wojciechowski CL, Kantrowitz ER. 2005. Structure of the wild-type TEM-1 *β*-lactamase at 1.55 A and the mutant enzyme Ser70Ala at 2.1 A suggest the mode of noncovalent catalysis for the mutant enzyme. Acta Crystallogr D Biol Crystallogr 61:1072–1079. https://doi.org/10.1107/S0907444905014356.

21. Fakhar Z, Govender T, Maguire GEM, Lamichhane G, Walker RC, Kruger HG, Honarparvar B. 2017. Differential flap dynamics in L,D-transpeptidase2 from *Mycobacterium tuberculosis* revealed by molecular dynamics. Mol Biosyst 13:1223–1234. https://doi.org/10.1039/C7MB00110J.

22. Kim HS, Kim J, Im HN, Yoon JY, An DR, Yoon HJ, Min HK, Kim SJ, Lee JY, Han BW, Suh SW. 2013. Structural basis for the inhibition of *Mycobacterium tuberculosis* L,D-transpeptidase by meropenem, a drug effective against extensively drug-resistant strains. Acta Crystallogr D Biol Crystallogr 69:420–431. https://doi.org/10.1107/S0907444912048998.

23. Lavollay M, Dubee V, Heym B, Herrmann JL, Gaillard JL, Gutmann L, Arthur M, Mainardi JL. 2014. In vitro activity of cefoxitin and imipenem against *Mycobacterium abscessus* complex. Clin Microbiol Infect 20:O297–O300. https://doi.org/10.1111/1469-0691.12405.

24. Gonzalo X, Drobniewski F. 2013. Is there a place for *β*-lactams in the treatment of multidrug-resistant/extensively drug-resistant tuberculosis? Synergy between meropenem and amoxicillin/clavulanate. J Antimicrob Chemother 68:366–369. https://doi.org/10.1093/jac/dks395.

25. Fernandez-Hidalgo N, Almirante B, Gavalda J, Gurgui M, Pena C, de Alarcon A, Ruiz J, Vilacosta I, Montejo M, Vallejo N, Lopez-Medrano F, Plata A, Lopez J, Hidalgo-Tenorio C, Galvez J, Saez C, Lomas JM, Falcone M, de la Torre J, Martinez-Lacasa X, Pahissa A. 2013. Ampicillin plus ceftriaxone is as effective as ampicillin plus gentamicin for treating *Enterococcus faecalis* infective endocarditis. Clin Infect Dis 56:1261–1268. https://doi.org/10.1093/cid/cit052.

26. Soroka D, Dubee V, Soulier-Escrihuela O, Cuinet G, Hugonnet JE, Gutmann L, Mainardi JL, Arthur M. 2014. Characterization of broad-spectrum *Mycobacterium abscessus* class A *β*-lactamase. J Antimicrob Chemother 69:691–696. https://doi.org/10.1093/jac/dkt410.

27. Soroka D, Ourghanlian C, Compain F, Fichini M, Dubee V, Mainardi JL, Hugonnet JE, Arthur M. 30 December 2016. Inhibition of *β*-lactamases of

mycobacteria by avibactam and clavulanate. J Antimicrob Chemother https://doi.org/10.1093/jac/dkw546.

28. Lefebvre AL, Le Moigne V, Bernut A, Veckerle C, Compain F, Herrmann JL, Kremer L, Arthur M, Mainardi JL. 2017. Inhibition of the *β*-lactamase Bla$_{Mab}$ by avibactam improves the *in vitro* and *in vivo* efficacy of imipenem against *Mycobacterium abscessus*. Antimicrob Agents Chemother 61:e02440-16. https://doi.org/10.1128/AAC.02440-16.

29. Erdemli SB, Gupta R, Bishai WR, Lamichhane G, Amzel LM, Bianchet MA. 2012. Targeting the cell wall of *Mycobacterium tuberculosis*: structure and mechanism of L,D-transpeptidase 2. Structure 20:2103–2115. https://doi.org/10.1016/j.str.2012.09.016.

30. Brammer Basta LA, Ghosh A, Pan Y, Jakoncic J, Lloyd EP, Townsend CA, Lamichhane G, Bianchet MA. 2015. Loss of a functionally and structurally distinct L,D-transpeptidase, Ldt$_{Mts}$, compromises cell wall integrity in *Mycobacterium tuberculosis*. J Biol Chem 290:25670–25685. https://doi.org/10.1074/jbc.M115.660753.

31. Minor W, Cymborowski M, Otwinowski Z, Chruszcz M. 2006. HKL-3000: the integration of data reduction and structure solution—from diffraction images to an initial model in minutes. Acta Crystallogr D Biol Crystallogr 62:859–866. https://doi.org/10.1107/S0907444906019949.

32. McCoy AJ. 2007. Solving structures of protein complexes by molecular replacement with Phaser. Acta Crystallogr D Biol Crystallogr 63:32–41. https://doi.org/10.1107/S0907444906045975.

33. Terwilliger TC, Grosse-Kunstleve RW, Afonine PV, Moriarty NW, Zwart PH, Hung LW, Read RJ, Adams PD. 2008. Iterative model building, structure refinement and density modification with the PHENIX AutoBuild wizard. Acta Crystallogr D Biol Crystallogr 64:61–69. https://doi.org/10.1107/S090744490705024X.

34. Afonine PV, Grosse-Kunstleve RW, Echols N, Headd JJ, Moriarty NW, Mustyakimov M, Terwilliger TC, Urzhumtsev A, Zwart PH, Adams PD. 2012. Towards automated crystallographic structure refinement with phenix.refine. Acta Crystallogr D Biol Crystallogr 68:352–367. https://doi.org/10.1107/S0907444912001308.

35. Emsley P, Cowtan K. 2004. Coot: model-building tools for molecular graphics. Acta Crystallogr D Biol Crystallogr 60:2126–2132. https://doi.org/10.1107/S0907444904019158.

36. Thomsen R, Christensen MH. 2006. MolDock: a new technique for high-accuracy molecular docking. J Med Chem 49:3315–3321. https://doi.org/10.1021/jm051197e.

37. Silva JR, Govender T, Maguire GE, Kruger HG, Lameira J, Roitberg AE, Alves CN. 2015. Simulating the inhibition reaction of *Mycobacterium tuberculosis* L,D-transpeptidase 2 by carbapenems. Chem Commun (Camb) 51:12560–12562. https://doi.org/10.1039/C5CC03202D.

38. Gavan TL, Town MA. 1970. A microdilution method for antibiotic susceptibility testing: an evaluation. Am J Clin Pathol 53:880–885. https://doi.org/10.1093/ajcp/53.6.880.

39. Desmond E. 2011. Susceptibility testing of mycobacteria, nocardiae and other aerobic actinomycetes. M24-A2. Clinical and Laboratory Standards Institute, Wayne, PA.

40. Hsieh MH, Yu CM, Yu VL, Chow JW. 1993. Synergy assessed by checkerboard. A critical analysis. Diagn Microbiol Infect Dis 16:343–349. https://doi.org/10.1016/0732-8893(93)90087-N.